Chapter 5

PHOTOMETRIC COMPONENTS IN DISK GALAXIES

5.1 Introduction

There are various properties of galaxies that can be used in comparing our Galaxy to external ones and a large number of these will be used in these lectures to see where the Galaxy we live in fits into the variety we observe among such objects in the Universe. This in itself is justification enough to make such comparative studies. However, there is a second, possibly more important reason and that is that by investigating properties of external galaxies we may be able to better interprete observations in our own stellar system, where our internal position is sometimes a major disadvantage. The way in which I will set up my lectures in this course will be to start out by describing what observations can be done in galaxies and how these are performed. Then I will review the findings of such studies, see what relevant observations are available for our Galaxy and then compare these two sets. I will start out with the distribution of stars, as revealed by studies of surface photometry. Since our Galaxy is a spiral galaxy, I will in general not describe elliptical galaxies. Distances are based on a Hubble constant of 75 km s^{-1} Mpc^{-1}. A related review in the Saas-fee series is the one by Kormendy (1982).

5.2 Methods of surface photometry

The classical technique is photographic surface photometry. The basic principle is simple: One takes a photographic exposure and scans the relevant part of the plate to provide a digital record. It is no surprise that this has been possible on a large scale only since the seventies, when fast and accurate scanning machines were being built and large computers

became available to control the scanning equipment and to perform the off-line data reduction. It should be noted however, that this kind of work does stem from earlier decades, but the point is that it could not be done on a large scale. Although notable exceptions do exist, most of these old studies provided a luminosity profile along a few axes, usually of course the minor and major axis. Another reason for the advent in the seventies must have been the availability of high-contrast, fine-grained emulsions such as the IIIa series of Kodak, that made it possible to work down to fainter levels and generally improve the accuracies.

The digital matrix, that makes up the recording of the photographic densities over the galaxy and its surroundings, often amounts to 512^2 or 1024^2 picture elements ("pixels") and sometimes more. The photographic density simply expresses the amount of light that emerges from the plate, when a light source is made to shine through it. It is on a logarithmic scale, such that 0.0 stands for 100%, 1.0 for 10%, etc. Usually densities can be measured reliably up to values of 3 or 4. The procedure to arrive at these is to calibrate the scanning machine with a set of filters of known density. The reduction consists of two steps. First the level of background density must be determined. This is usually done by fitting a two-dimensional low-order polynomial to a region surrounding the galaxy, where one iteratively corrects for the field stars. Next a conversion from photographic density to intensity must be performed.

For this purpose the "characteristic curve" must be known, which expresses the relation between the logarithm of the exposure (incident intensity times exposure time) and density. During or shortly after exposure on the telescope therefore a set of spots of known exposure ratio or a wedge along which the exposure varies in a known manner is imprinted on a separate part of the plate. It is vital that this is done with the same wavelength dependence as prescribed by the telescope–filter combination and with the same exposure time. The latter is because of low intensity reciprocity failure, which says that at faint levels, such as from the night sky, a particular exposure results in a different density than at bright levels. The linear part of the characteristic curve between under- and over-exposure is often described by the slope γ, which is about 3 for Kodak IIIa-J or IIIa-F plates.

With this curve it is possible to convert the density of galaxy+sky and of sky alone into an intensity and hence in a ratio of galaxy surface brightness to that of sky during the observations. To determine the absolute values of surface brightness (the zero-point) one compares the integrated magnitude of (a part of) the galaxy to that determined by photoelectric measures. The main uncertainty usually comes from the background determination; every plate is usually prepared by "baking" for a few hours in a nitrogen or nitrogen/hydrogen environment at something like 65°C and this and other inhomogeneities result in non-uniformity of the emulsion response. For practical purposes this limits photometry from a single plate to about 5 magnitudes fainter than sky, although

fainter work can be done from repeated exposures. Due to the limited dynamic range of a plate a combination of short and long exposures is necessary for a single galaxy to completely determine its surface brightness distribution.

It is an incorrect believe that luminosity scales are in practice often seriously wrong. The reality is, that characteristic curves can be determined rather easily to high accuracy. Furthermore, as to my knowledge first pointed out by Ivan King, at faint levels magnitude scales are independent of the value of γ, which can be seen as follows. The characteristic curve in its linear part can be written as

$$D = \gamma \log E, \tag{5.1}$$

where D is density and E exposure. If surface brightness μ is expressed in magnitudes per square arcsecond, it follows that

$$D_{\rm sky} = -\left(\frac{\gamma}{2.5}\right)\mu_{\rm sky} + \text{constant}. \tag{5.2}$$

If the density of sky + object is $D_{\rm sky} + \Delta D$ and if $\Delta D \ll D_{\rm sky}$, then

$$\log(\Delta D) = \log\left(\frac{\gamma}{\ln 10}\right) + \frac{(\mu_{\rm sky} - \mu)}{2.5}. \tag{5.3}$$

Now for two faint regions in the outer parts of the galaxy the difference in surface brightness in mag arcsec^{-2} is

$$\mu_1 - \mu_2 = 2.5 \log\left(\frac{\Delta D_2}{\Delta D_1}\right) \tag{5.4}$$

and independent of γ. The basic reason for this is of course that magnitudes are ratio's of intensity. Clearly the background subtraction remains vital, but the intensity scale is correct regardless of the density to intensity conversion.

In recent times it has been possible to do digital recording at the telescope with photon counting detectors such as in particular CCD's (Charge Coupled Devices). The data reduction here has some special features not encountered with photographic plates (see also Okamura, 1988). The detectors suffer from sensitivity variations due to electronic and optical effects during the exposure and noise during the transfer of the data from the chip to disk storage (read-out noise). The general noise level is determined from a so-called bias frame that has collected data for the same period as the observations, but with the camera shutter closed. This is subtracted from the raw data, but does of course leave some noise. Then there are cosmetic effects, such as in particular "fringing" (interference in the chip) and cosmic ray events, while columns can be affected by a bright star in the field. These are removed by linear interpolations across the relevant pixels. Then there is the serious problem of sensitivity variations from pixel to pixel, which is calibrated by

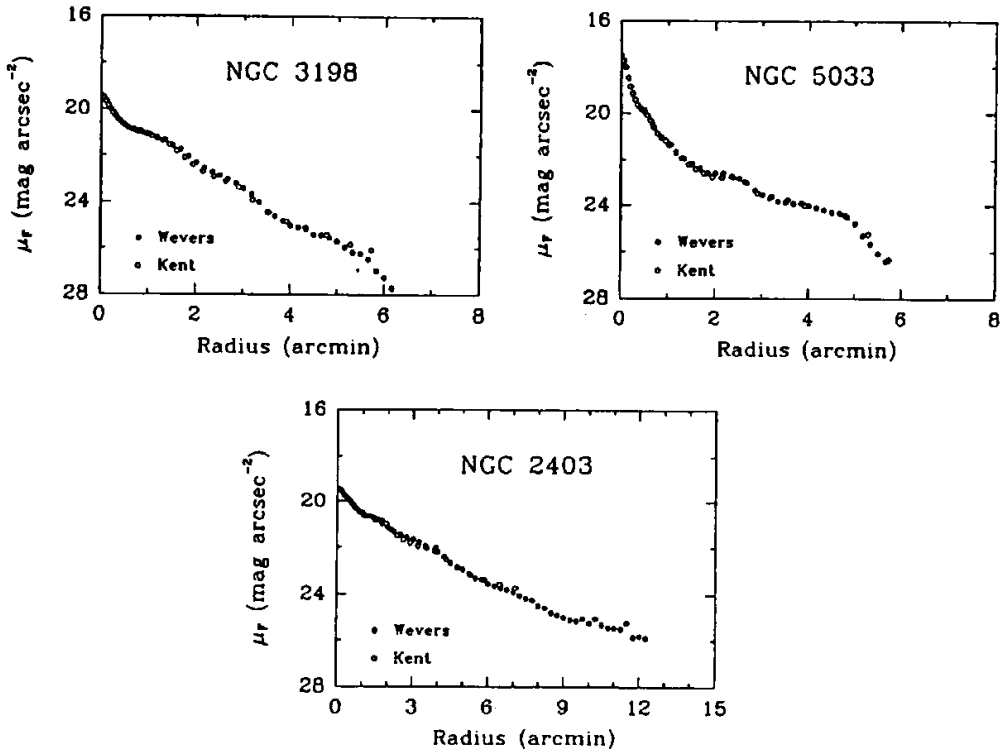

Figure 5.1: The radial surface brightness profiles of three spiral galaxies determined by photographic photometry (Wevers et al., 1986) and from CCD photometry (Kent, 1987). The vertical scale is in the F-band of Wevers et al. and the data from Kent have been scaled from the r-band to the F-band. The largest difference is 0.2 mag. From Begeman (1987).

dividing the observed frame by a flat field exposure on a uniformly illuminated screen in the dome or the twilight sky. Flat-fielding and read-out noise are the most important limitations. Calibration of the photometric scale is usully done by making exposures during the night on fields with standard stars.

At present the most serious shortcoming of CCD's is the small field of view due to the limited size of the commercially available chips. To some extent this can be overcome by placing a few CCD's next to each other such as in the "four-shooter" at the Palomar 5–m telescope. Alternatively, one may take overlapping exposures and combine these later. Current industrial developments may make larger chips accessible soon. The great advantages of photon-counting detectors are the good quantum efficiency, the large dynamic range and the fact that digital data are provided right at the telescope. The linearity is often quoted also as an advantage. However, the response of photographic

plates can be calibrated in a straightforward and reliable way, while —as shown above— at faint levels a magnitude scale is provided independent of the slope of the characteristic curve. The necessity to digitize the plates, the limited dynamic range and the unavoidable non-uniformities remain the most serious limitations and for study of individual objects of limited angular extent, photon counting will be the technique to use. The high quantum efficiency does make the use of CCD's on small telescopes possible and in that case a reasonable field of view of 10 or more arcmin can be obtained.

Published photographic and CCD observations now are in excellent agreement. Begeman (1987) has compared radial profiles from photographic photometry by Wevers et al. (1986) and CCD work by Kent (1987) for three spiral galaxies (see fig. 5.1). Not only are the general shapes in excellent agreement, but also features in the profiles reproduce between the two techniques. The largest individual difference is only 0.2 mag. Kent's profiles reach into the centre, where the photographic plates were overexposed, but mainly due to angular size the CCD data do not go as far out in galactocentric radius. The sky background for these data is about 21 mag arcsec^{-2}, so it can be seen that the agreement continues to a level of 5 mag below sky or 1% of the sky surface brightness.

5.3 Bulge and disk luminosity distributions

Because of the brighter surface brightness, the first attempts to measure light profiles in external galaxies were performed on bulges of spiral galaxies and on ellipticals. The oldest reference to my knowledge is Reynolds (1913), who presented a radial light profile along the major axis of the bulge ("globular nucleus") of M31. It was based on photographic exposures of up to 100 minutes on a 28–inch reflector. It is interesting that Reynolds in his paper argued on the basis of his photographs that M31 is unlikely to be a "very distant galaxy of stars" and that "the light of the nebula is derived in some measure from a central star which is too much involved in nebular matter to be visible as such". He immediately tried to fit the radial profile with an empirical function, and found a satisfactory one to be $(x+1)^2 y =$ constant with x radial distance and y the "light ratio" (surface brightness on a linear scale without known zero-point). Reynolds' measurements and his fit are shown in fig. 5.2. His largest radial extent is 6.0 mm or 6.9 arcmin. From modern surface photometry (Walterbos and Kennicutt, 1987) we know that at this radius the surface brightness is about 21 B-mag arcsec^{-2}. The fitted function was later also used by Hubble in the form $I(R) = I_o(R+a)^{-2}$.[1]

The most successful empirical formula was formulated by de Vaucouleurs (1948) and is usually referred to as the "$R^{1/4}$-law". It appears to be able to represent actual profiles

[1]Here and in the following I will denote surface brightness on a linear scale, such as $L_\odot$ pc^{-2} with the symbol I and use μ when the unit is mag arcsec^{-2}.

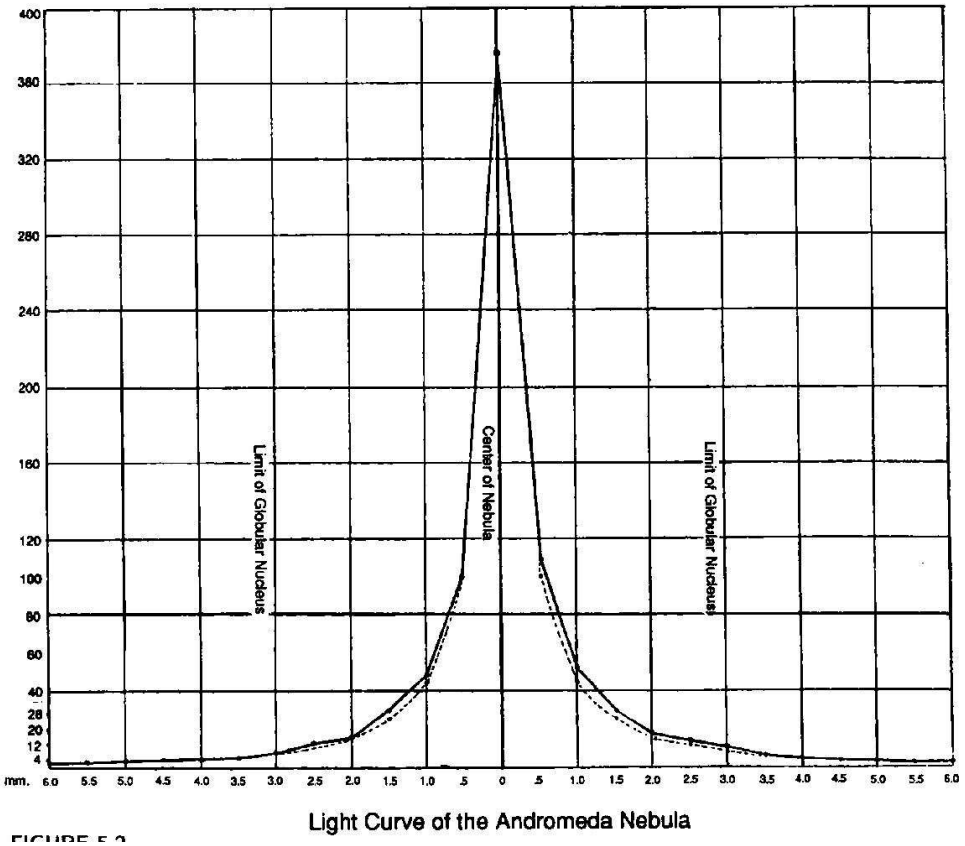

Figure 5.2: The earliest observed distribution of surface brightness in the bulge of M31. The vertical scale is linear in relative units and the horizontal scale is in mm on the plate, where 1 mm corresponds to 69 arcsec. The dashed lines are fits with Reynolds' quadratic form (see text). From Reynolds (1913).

in bulges and ellipticals over a very wide range in surface brightness. Its equation is

$$\log\left\{\frac{I(R)}{I_{\rm e}}\right\} = -3.3307\left[\left(\frac{R}{R_{\rm e}}\right)^{1/4} - 1\right]. \tag{5.5}$$

Here $R_{\rm e}$ is the effective radius that encloses half the total light and $I_{\rm e}$ the surface brightness at that radius. The central surface brightness then becomes $\mu(0) = \mu_{\rm e} + 8.3268$. The corresponding total luminosity is

$$L = 7.215\,\pi I_{\rm e} R_{\rm e}^2 (b/a), \tag{5.6}$$

where b/a is the apparent axis ratio.

The wide applicability is surprising from a physical point of view. The corresponding volume luminosity density cannot be given analytically. Young (1976) has given tables of various properties, including the space luminosity density. Also he gives approximations at small and large radii, where the latter one is most useful for practical applications. With total luminosity L in $L_\odot$, R_e in pc, the density at radius R (also in pc) is for the spherical case in $L_\odot$ pc^{-3}

$$L(R) = 52.19 \left(\frac{L}{R_\mathrm{e}^3}\right) \left(\frac{R}{R_\mathrm{e}}\right)^{-7/8} \exp\left\{-7.67 \left(\frac{R}{R_\mathrm{e}}\right)^{1/4}\right\}. \tag{5.7}$$

For a flattened system with axis ratio (b/a), R should be replaced by α, where $\alpha^2 = R^2(b/a)^2 + z^2$.

A close, alternative surface brightness law, that does have a manageable representation of the space distribution has been given by Jaffe (1983) in order to compare to dynamical models. It has the volume density distribution

$$L(R) = \frac{1}{4\pi} \left(\frac{R_{.5}}{R}\right)^2 \left[1 + \left(\frac{R}{R_{.5}}\right)\right]^{-2}, \tag{5.8}$$

where $R_{.5} = 1.311 R_\mathrm{e}$ encloses half the total emitted light in space and the total integrated luminosity has been normalized to unity. The projected surface brightness can be calculated analytically, as well as such properties as gravitational potential, etc. Binney (1982) has devised a dynamical model that is in a sense "isothermal" and also corresponds closely to observed light profiles that can be fitted to the $R^{1/4}$-law. In his model the distribution function of stars is expressed as a function of the binding energy E and is given by the Boltzmann formula $N(E) = N_\mathrm{o} \exp(-\beta E)$, where $\beta = 2.08 R_\mathrm{e}/GM$ with M the total mass.

For ellipticals and with less success also for bulges there has been some use of the King-model (King, 1966), in which the starting point has been a distribution function of the particles, that is isothermal and in which all particles have the same mass. This distribution function is a truncated Maxwellian. Wilson (1975) extended these models to include rotation. More recently, Jarvis and Freeman (1985a,b) have constructed similar dynamical models for bulges in which rotation has been included, while the effects of the disk potential have also been taken into account. Their distribution function is

$$f(E, J) = \alpha \left[\exp(-\beta E) - \exp(-\beta E_\mathrm{o}) \right] \exp(\gamma J), \tag{5.9}$$

where E ($< E_\mathrm{o}$) is the energy per unit mass and J the component of angular momentum per unit mass parallel to the axis of symmetry. Models with $\gamma = 0$ are King models. Assuming constant mass-to-light ratio's M/L, they were able to fit such models to the surface brightness distribution and stellar kinematics of actual bulges of a few early type

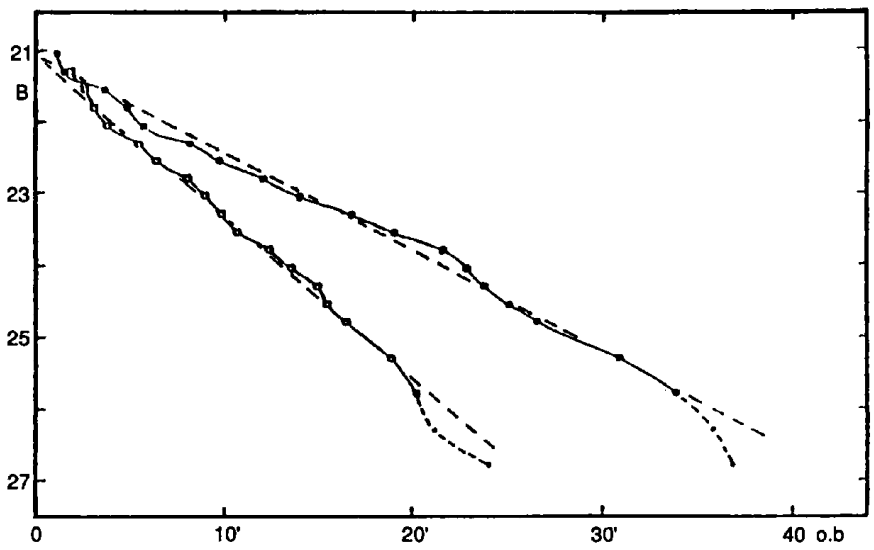

Figure 5.3: The surface brightness distribution of the disk of the Local Group Sc galaxy M33. The two curves show the distributions measured along the minor and major axes separately. The dashed lines indicate exponentials. From de Vaucouleurs (1959b).

systems, where the light distribution is dominated by that of the bulge. Data show that bulges are consistent with their being isotropic oblate spheroids in which flattening is mostly due to rotation.

The description of the radial surface brightness distribution in disks followed that of bulges and ellipticals by about three decades. This is an understandable result of the much fainter surface brightness of the disks. There is one simple law for the radial distribution of surface brightness, namely that of the exponential disk:

$$I(R) = I_{\rm o} \exp\,(-R/h). \tag{5.10}$$

The parameter h is usually referred to as the disk scalelength. The integrated magnitude is

$$L = 2\pi h^2 I_{\rm o}. \tag{5.11}$$

The exponential law was first described in an unpublished Harvard thesis based on observations of M33. A short report is available in Patterson (1940) and a plot of the data appears in the extensive description of light distributions in galaxies by de Vaucouleurs (1959a, his fig. 10). The first detailed work was performed by de Vaucouleurs in a series op papers in the late 1950's that involved the suitable members of the Local Group: LMC, M31 and M33. This fundamental work established once and for all that exponentials are the rule and occur in Sb, Sc and Irregular galaxies. De Vaucouleurs' (1959b) exponential

light profile of the disk of M33 is reproduced from the original paper in fig. 5.3. Note that the data reach a level of about 27 B-mag arcsec^{-2}, which is not much brighter than is attainable today in such studies. The two curves show the major and minor axis profiles separately.

Many studies have in the mean time confirmed the universal applicability of the exponential as a fitting function. It should however be noted, that in all galaxies for which an exponential has been fitted to the disk surface brightness profile there are important, non-local deviations from the fit at a level of a few tenths of a magnitude, while often the fit can be performed over a few magnitudes (about e-foldings) interval in the first place (e.g. van der Kruit, 1987a, see also fig.5.1). The reason for the last point is that often the bulge dominates the inner parts and then there is little fall-off in surface brightness left before reaching the noise introduced by the sky background. This means that the exponential is convenient to use because of its simplicity as well as because of the limited range over which surface brightness profiles can be determined. The significance of the facts just mentioned is that one should be hesitant to attach too much physical meaning to the exponential nature. I will discuss the distribution of the central surface brightness and the scalelength later in this course (see also van der Kruit, 1987a); however, here I already note that Freeman (1970) found that large spiral galaxies appear to display a remarkably small range in extrapolated central (face-on) surface brightness, namely 21.65±0.30 B-mag arcsec^{-2}.

Disks do have a finite thickness. The three-dimensional structure therefore requires a description of the vertical distribution. Van der Kruit and Searle (1981a) proposed to use the formula for the (locally) self-gravitating, isothermal sheet for this, so that the full description becomes

$$L(R,z) = L(0,0)\,\exp\,(-R/h)\mathrm{sech}^2(z/z_\mathrm{o}). \tag{5.12}$$

The face-on surface brightness follows from

$$I(R) = 2z_\mathrm{o}L(R,0) \tag{5.13}$$

and the vertical scale parameter z_o relates to the surface density $I(R)(M/L)$ and the velocity dispersion $\langle V_\mathrm{z}^2\rangle^{1/2}$ as

$$\langle V_\mathrm{z}^2\rangle = \pi G I(R) z_\mathrm{o}(M/L). \tag{5.14}$$

The reason for choosing the isothermal sheet was the observation in the solar neighborhood (e.g. Wielen, 1977), that stars that have ages above a few Gyrs all have roughly the same velocity dispersion, so that the mix of disk stars should be dominated — at least moderately far from the plane — by essentially a single stellar population with a single velocity dispersion. This component is the "old disk population" in terms of the popula-

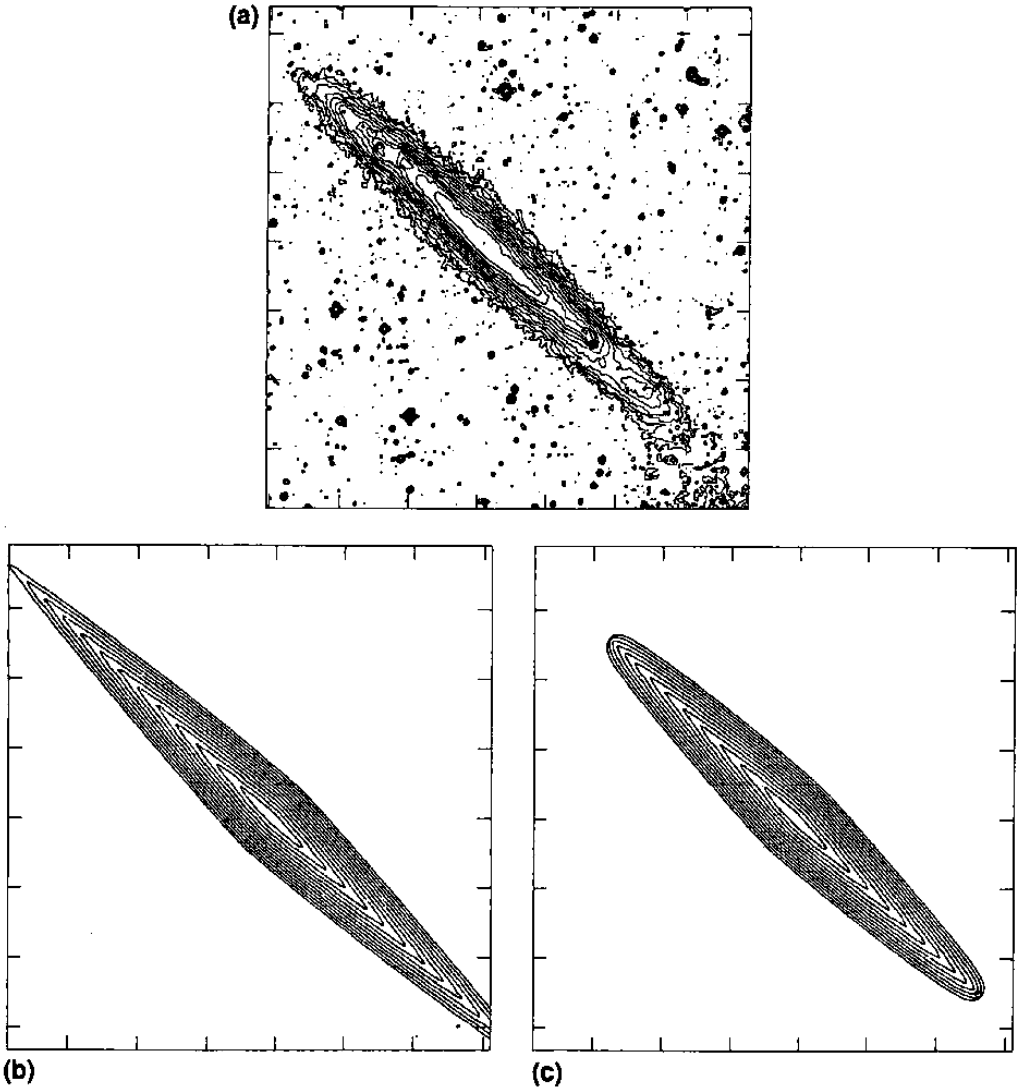

Figure 5.4: Optical isophotes of the edge-on, pure disk galaxy NGC 4244. (a) The observed contour map after subtraction of the responses of some foreground stars, that were superimposed on the image of the galaxy. The contours are spaced by 0.5 mag and the faintest contour is at about 27.5 B-mag arcsec^{-2}. (b) Isophote map of an edge-on model disk with an exponential luminosity distribution in the radial direction and that of an isothermal sheet approximation in the vertical direction. Although the inner isophotes are fitted very well (except in the plane due to dust and young stars) the model extends to larger galactocentric distances than the observations. (c) The same model as in (b), but with a sharp edge. The observations are now represented very well by the model. From van der Kruit and Searle (1981a).

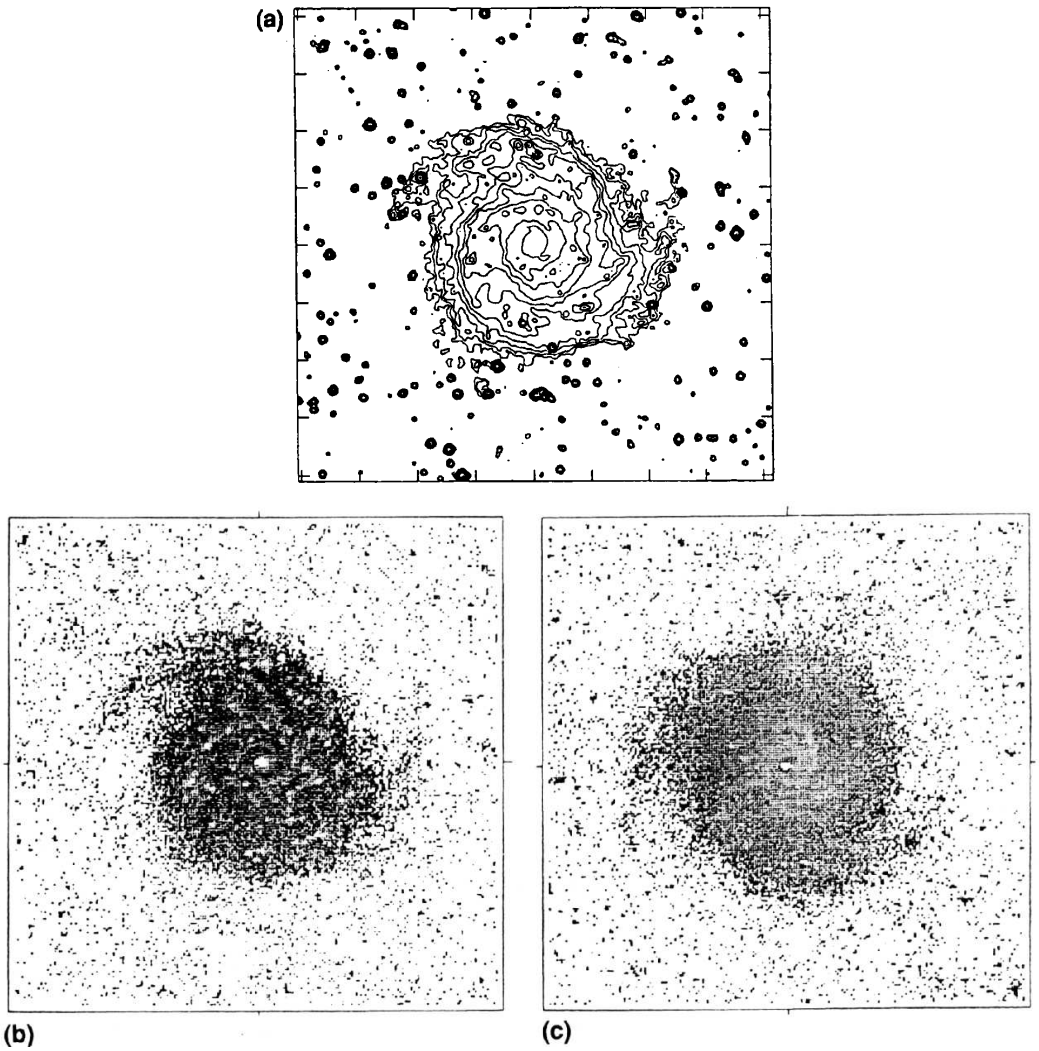

Figure 5.5: (a) Isophote map of the face-on spiral NGC 628 after removal of some foreground stars. The contours are spaced by 0.5 mag and the faintest contour is at 26.5 B-mag arcsec^{-2}. (b) Grey-scale representation of the color distribution in NGC 628 in pixels of 5 arcsec. The dark pixels have $(U-B)$ about 0.65 and the empty ones -0.85. Area's in which the surface brightness was too faint or where one of the plates was overexposed (in the nucleus and on bright field stars) were also left white. Note that the spiral arms show up very well due to the blue colors of the HII regions. (c) The same as in (b), but now the range is $(B-V)$ from 1.5 (dark) to 0.3 (white). The effect of the HII regions is now much less pronounced and there appears a fairly uniform color across the disk. Fig. 5.5a is from Shostak and van der Kruit (1984) and the other two are not previously published figures from that study.

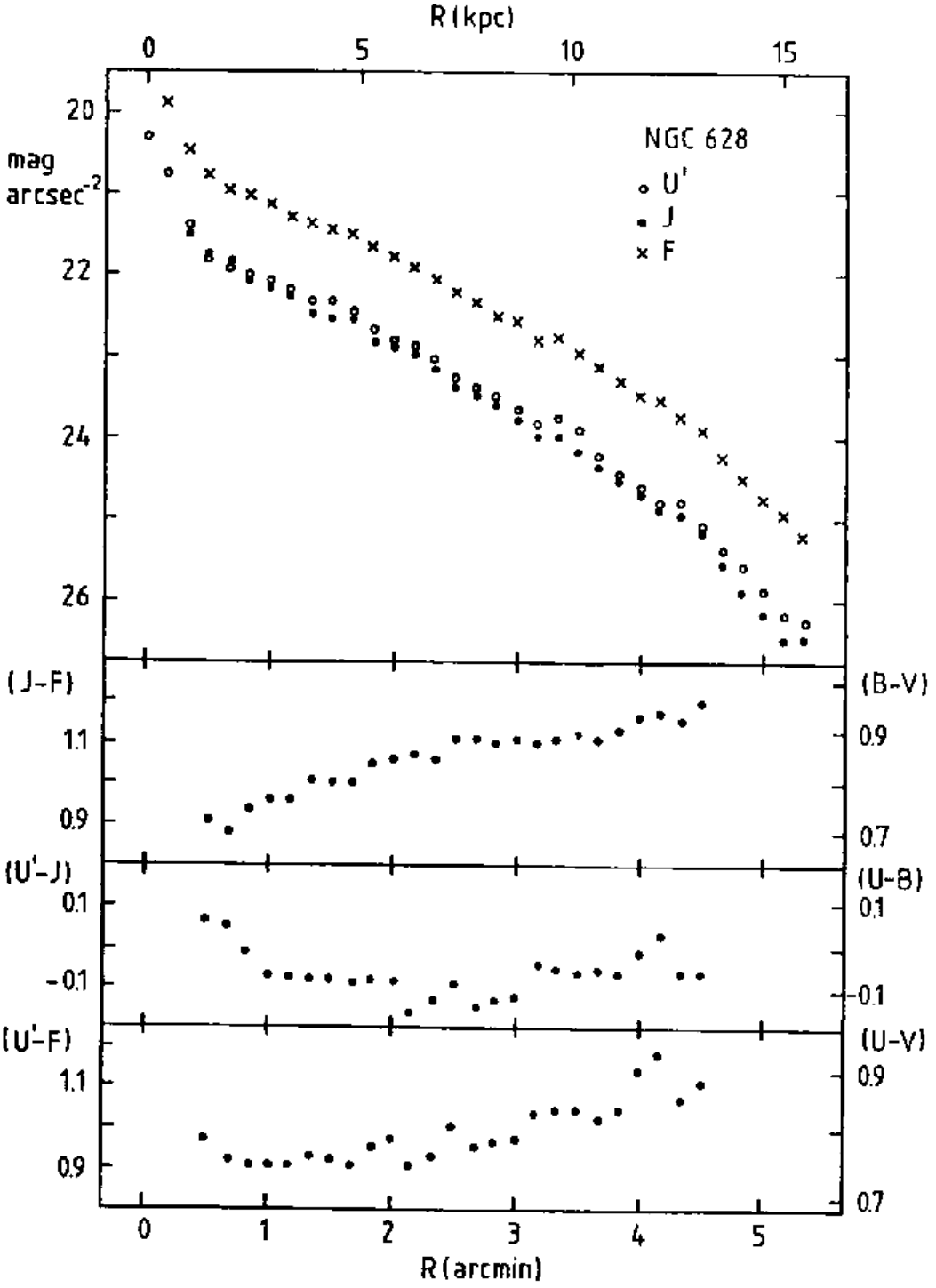
R (kpc)
0
5
10
15
20
22
24
26
mag
arcsec^{-2}
NGC 628
U'
J
F
(J-F)
1.1
0.9
(B-V)
0.9
0.7
(U'-J)
0.1
-0.1
(U-B)
0.1
-0.1
(U'-F)
1.1
0.9
(U-V)
0.9
0.7
0
1
2
3
4
5
R (arcmin)

Figure 5.6: Radial profiles of surface brightness and color in the disk of NGC 628. At the top are three profiles in U' (about standard U), J (from IIIa-J plates and about B) and F (from IIIa-F plates and somewhat redder than V). Note the exponential declines and the absence of a sharp truncation. At small R the increase due to the small bulge can be seen. The bottom three profiles are the three color distributions. The colors have been translated in $(U-B)$ and $(B-V)$ at the right. From Shostak and van der Kruit (1984).

tion scheme put forward at the famous "Vatican Symposium" on stellar populations in 1957. Furthermore, earlier observations (e.g. van der Kruit, 1979) had indicated that disks have roughly exponential z-profiles with the scale parameter independent of galactocentric distance. The latter agrees with the isothermal disk, because the sech^2 has the property that it approaches an exponential with e-folding $z_\mathrm{o}/2$ for large z:

$$\mathrm{sech}^2(z/z_\mathrm{o}) = 4\,\exp\,(-2z/z_\mathrm{o}) \quad \text{for} \quad z/z_\mathrm{o} \gg 1. \tag{5.15}$$

Actual fits of the proposed three-dimensional distribution to photometry of edge-on galaxies with little or no bulge confirmed the applicability and in particular the remarkable property that z_o is constant with R (see fig. 5.4). It should be stressed that the description refers only to the old disk population and ignores effects from young population I stars and dust.

It was also found earlier that disks have rather sharp outer edges or truncations (van der Kruit, 1979; see also fig. 5.4). From a sample of 7 edge-on spirals, van der Kruit and Searle (1982a) found that this radius R_max occurs at 4.2 ± 0.6 radial scalelengths h. This was not known from luminosity profiles of inclined or face-on systems and van der Kruit (1988) has proposed that this is the result of relatively small deviations from circular symmetry in the stellar disks. This can for example be seen in the isophote map of the face-on spiral NGC 628 (fig. 5.5a), where the outer three isophotes are much more closely spaced than the inner ones. On the other hand, these isophotes do deviate from pure circles. These deviations correspond to variations in R_max of order 10% with azimuthal direction. As a result, radial profiles obtained by azimuthal averaging of the light distribution fail to show the sharp declines. Beyond the "truncation radius" the radial e-folding of the light distribution drops to values generally less than 1 kpc.

In fig. 5.5 an example of surface photometry of a face-on spiral with very little bulge is given, using the ScI galaxy NGC 628. Also color distributions are shown. The spiral structure outlined by the HII regions shows up very well in particular in $(U-B)$. From such data the radial profiles can be determined by azimuthal averaging of the intensities. This is shown in fig. 5.6. Note the absence of a sharp edge, although as pointed out above these can be seen from the contour spacings in the maps, but have been smoothed out by the procedure. There is no significant color variation in $(U-B)$ with radius and a

reddening is observed in $(B-V)$ with an amplitude of 0.25 mag. This is marginally significant. The question of color variations has been investigated in a sample of 21 galaxies by Wevers (1984; see also Wevers et al. 1986). The result is that a few radial color gradients are indeed seen, but there certainly is no systematic trend in these, while in most disks there is no evidence at all for radial color gradients. This observation is of great interest, because it seems to indicate that at all radii there is the same mix of stars of various ages and therefore no radial gradient in the time-dependence of the star formation rate.

5.4 Component separation in disk galaxies

The luminosity laws described above make it possible to perform a decomposition of a radial surface brightness profile of a spiral galaxy into a disk and bulge component. The usual procedure is to select first on the profile of that region that appears dominated by the exponential disk and estimate initial parameters for μ_o and h. Subtraction of this initial disk model then gives rise to a first guess of the parameters μ_e and R_e for the bulge. Least-squares or χ^2 minimization techniques are then used to find a final solution to the observed profile by variation of the four parameters. Of course, this method relies heavily on the a priori assumption that these fitting functions are exact descriptions of the distributions within the two components.

For most galaxies the procedure works quite satisfactorily. Schombert and Bothun (1987) have recently studied it in detail both on artificial light profiles (with realistic noise introduced) and those of actual galaxies. They find that for the bulge component, errors in effective radius and surface brightness occur in a way that conserves the total luminosity and these errors are of course worse in systems with small bulges. In galaxies strongly dominated by the bulge, the procedure tends to underestimate the disk central surface brightness by 0.2 to 0.3 mag and overestimate the scalelength by 10 to 30%. fig. 5.7 illustrates these effects.

In fig. 5.8 a few examples of component decomposition in actual CCD luminosity profiles are given, also from Schombert and Bothun. The first thing to notice is the fact, that the bulges dominate usually only in the very inner region, even in the relatively strong bulge of NGC 2565. Another feature of the $R^{1/4}$-law is that at large radii it will eventually always dominate the disk contribution. Further it can be seen that disks seldom conform exactly to the exponential description in a detailed fashion. Most of this departure from a straight line in the plots is a result of structure in the disk, such as spiral arms or bars, but quite often it also is an intrinsic feature that is uncorrelated with such components. This stresses the limited value of the fitting function and the point made above that it would be wrong to attach too much physical significance to the exact exponential nature.

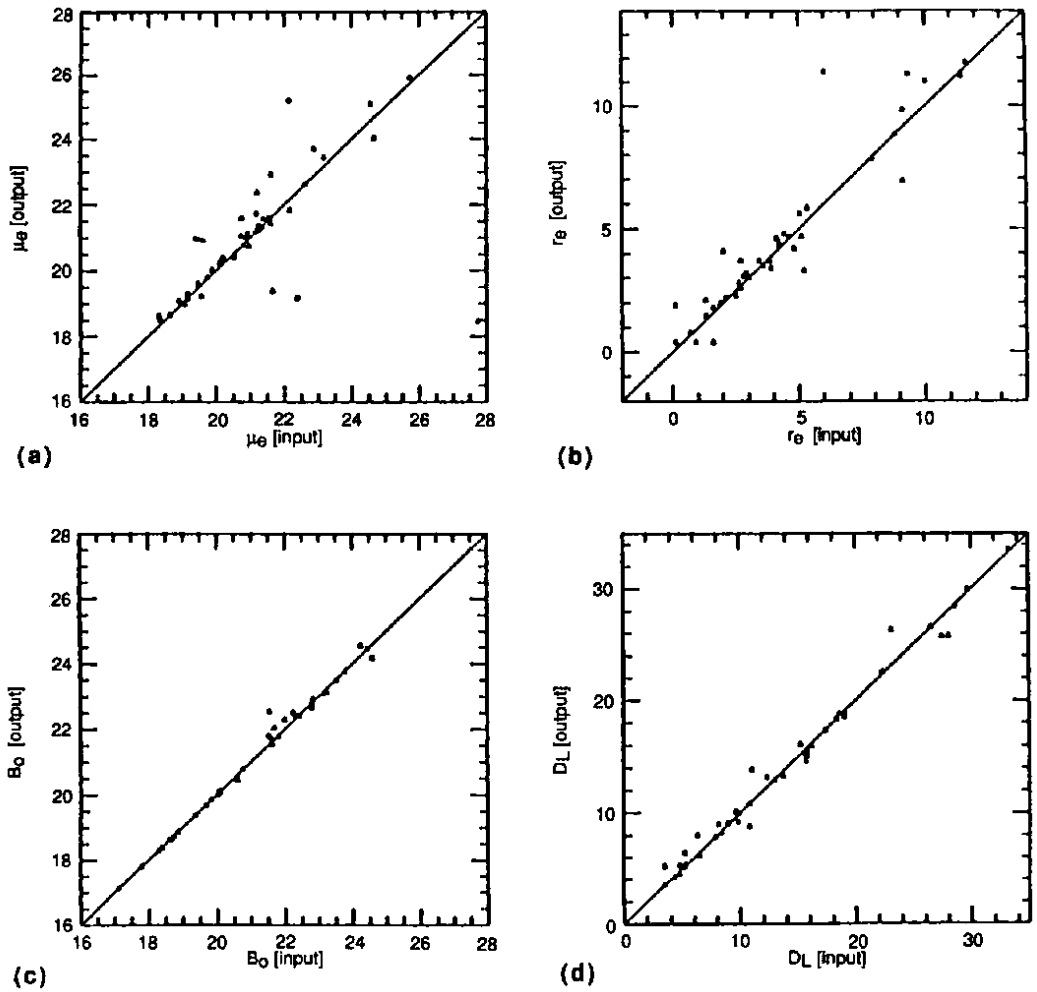

Figure 5.7: Results of component decomposition in artificial galaxy surface brightness profiles. The horizontal axes show the input parameters and the vertical ones those derived by the fitting procedure for the $R^{1/4}$-bulge in (a) and (b), respectively $\mu_{\rm e}$ and $R_{\rm e}$, and the exponential disk in (c) and (d), respectively $\mu_{\rm o}$ and h. From Schombert and Bothun (1987).

The reason for attempting component separation in the first place is that studies of our Galaxy have indicated that it — and therefore other spiral galaxies as well — can be described as fundamentally existing of two separate populations: halo and disk. In a first approximation these can be characterized by discretely different spacial distribu-

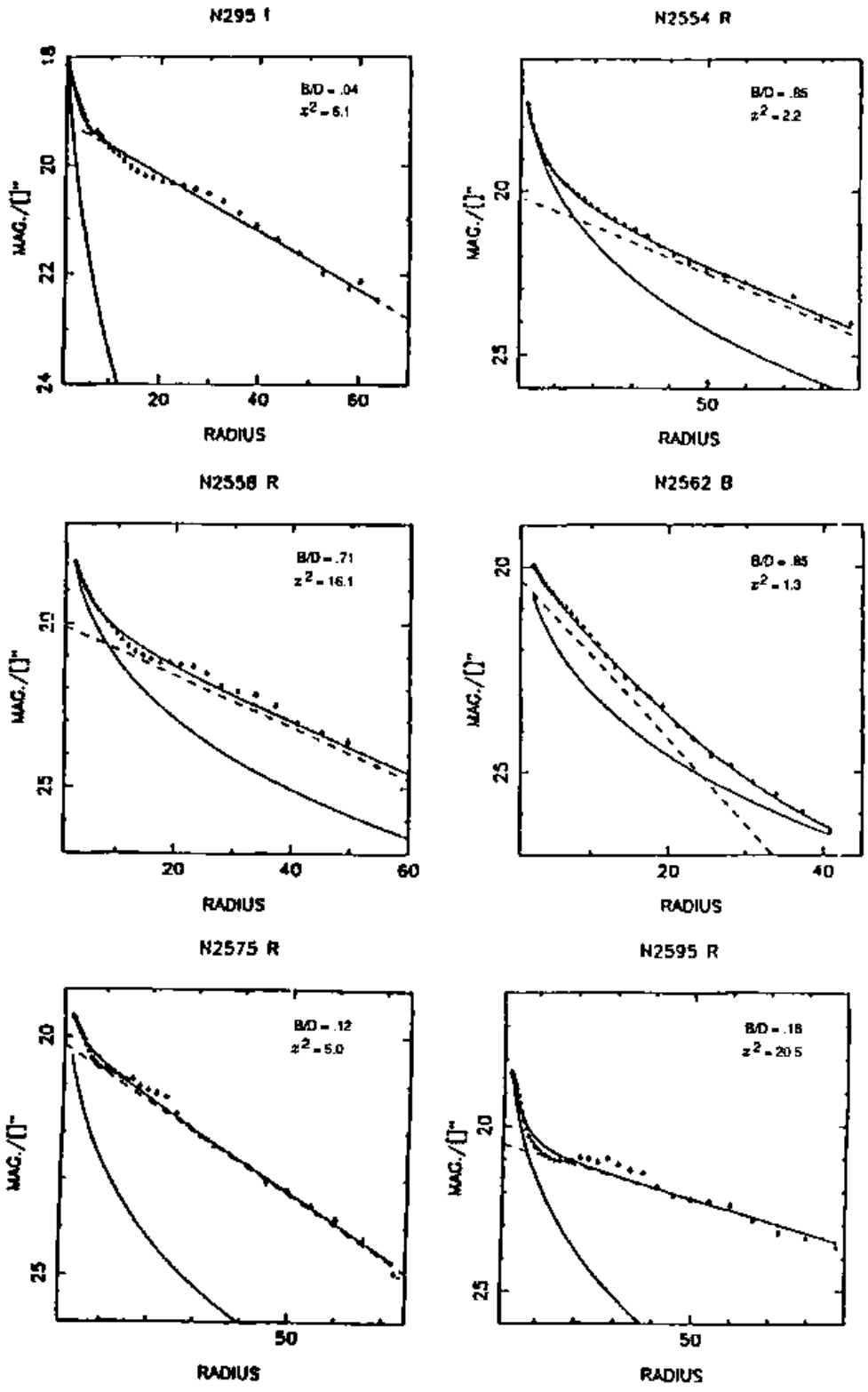
N295 I
B/D = .04
χ² = 6.1
MAG./[]"
RADIUS
N2554 R
B/D = .85
χ² = 2.2
MAG./[]"
RADIUS
N2558 R
B/D = .71
χ² = 16.1
MAG./[]"
RADIUS
N2562 B
B/D = .85
χ² = 1.3
MAG./[]"
RADIUS
N2575 R
B/D = .12
χ² = 5.0
MAG./[]"
RADIUS
N2595 R
B/D = .18
χ² = 20.5
MAG./[]"
RADIUS

Figure 5.8: Results of component separation in a few galaxies. The $R^{1/4}$-bulge, exponential disk and the sum of the two model components are all indicated. From Schombert and Bothun (1987).

tions, kinematics and distributions of stellar ages and of heavy element abundances. The reasonable success of decomposition of radial luminosity profiles confirms that this basic picture also applies to spiral galaxies in general. However, the question of possible discretely different spacial distributions in the sense of flattening is not yet addressed by these studies and for that purpose we need to look at edge-on galaxies, where there is a sizable part of the total solid angle that is covered by the bulge alone and vice versa.

As examples I will take two edge-on galaxies studied by van der Kruit and Searle (1981b, 1982b), namely the disk dominated galaxy NGC 891 and the bulge dominated system NGC 7814. As these studies also addressed color distributions, I will discuss this aspect at the same time. Fig. 5.9 illustrates the procedure for NGC 891. At the left we have the isophote map of the galaxy after subtraction of the responses of a large number of foreground stellar images. The regions away from the dust lane in the plane and the central bulge have been used to model the old disk population. The best fitting model, which is a that of an exponential, locally isothermal, truncated disk with constant thickness seen edge-on, is shown in the middle illustration. For a distance of 9.5 Mpc ($H_{\rm o}$ = 75 km s^{-1} Mpc^{-1}) the parameters are: $L(0,0) = 2.4\ 10^{-2} L_{\odot}$ pc^{-3} (in about the B-band), h = 4.9 kpc, $z_{\rm o}$ = 0.99 kpc and $R_{\rm max}$ = 21 kpc and the total old disk luminosity is then 6.7 10^9 $L_{\odot}$. At the right this model has been subtracted from the observations and the bulge remains. It turns out that the minor axis profile can be fitted well with an $R^{1/4}$-law with $R_{\rm e}$ = 2.3 kpc in the same band. The isophotes have a mean axis ratio of 0.6, but the outer ones are definitely flatter than the inner ones. The integrated luminosity then is 1.5 10^9 $L_{\odot}$. The old disk contains 82% of the light in old stars.

Fig. 5.10 illustrates the color data on NGC 891. At the left is the total light. Note that the dust lane is red (dark), but that in its center there are clear indications of the bluer young population I. At the right we see the bulge color distribution after disk subtraction. There is an obvious bluing towards larger radii. The color of the disk model is $(U-B) = 0.2$ and $(B-V) = 0.8$, which is indeed consistent with that of an old disk population. The color range in the observed part of the bulge is $(U-B) = 0.7$ to –0.1 and $(B-V) = 1.0$ to 0.7. These colors have zero-point uncertainties of about 0.2 mag and the color variation itself is uncertain by about 0.3 mag. The color gradient is most likely a result of a radial variation in metal abundance. This is the combined result of three possible effects: (1) For lower abundance the effective temperature on the giant branch increases. (2) For a lower metallicity there is among old populations a horizontal branch that reaches further towards blue colors (but beware of the so-called second parameter

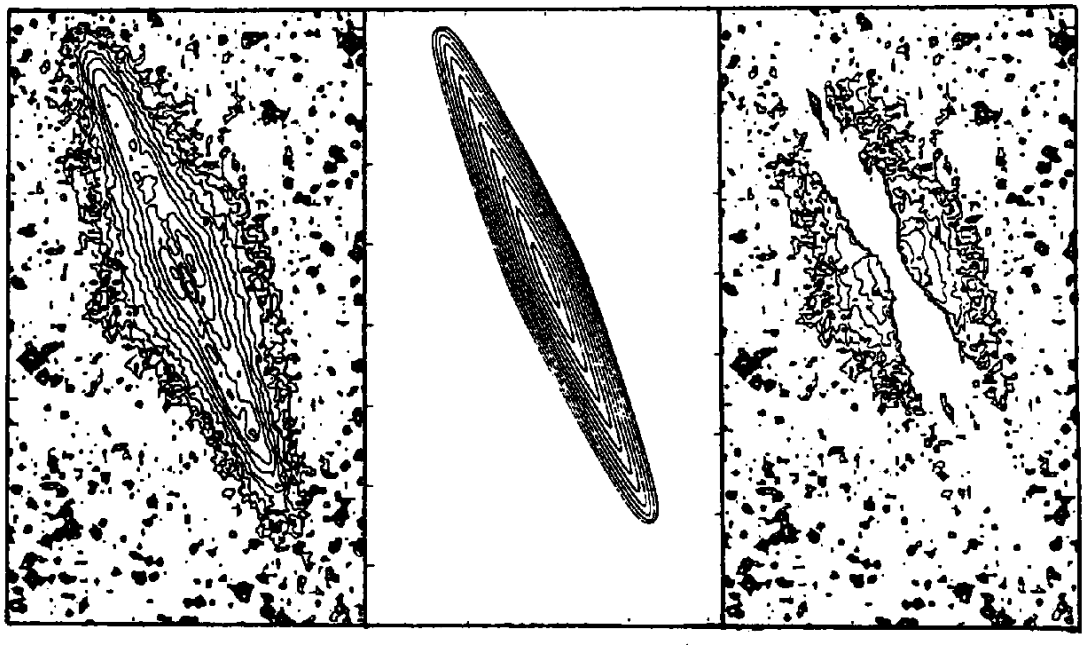

Figure 5.9: Isophote maps for NGC 891 in a band that is close to standard B. The faintest contour is at about 26.5 mag arcsec^{-2} and the interval is 0.5 mag. At the left we have the total galaxy light after subtraction of foreground stars, in the middle the model for the old disk population and at the right the light that remains after subtraction of the disk model from the observations. After van der Kruit and Searle (1981b).

effect in globular cluster HR-diagrams). (3) Line-blanketing, which is more severe at blue and UV wavelengths, is less effective in low abundance stars. The range of colors above is comparable to integrated colors of Galactic globular clusters and therefore indicates a similar metallicity range, say from [Fe/H] about -0.5 to -2 or so.

In fig. 5.11 the procedure is illustrated for NGC 7814. Here the bulge dominates and therefore a model is made for the bulge first. This model has an $R^{1/4}$ luminosity distribution and a uniform flattening of 0.57. In the B-band $R_{\rm e} = 2.2$ kpc and $\mu_{\rm e} = 22.1$ mag arcsec^{-2}; the total bulge luminosity then is 1.6 10^{10} $L_\odot$. The disk light remaining after subtraction of the bulge model from the observations is shown in the lower part. The central part is missing, because the plates were overexposed there in this photographic work. The crude parameters for the disk are $L(0,0) = 6.6\ 10^{-4}\ L_\odot$ pc^{-3}, $h = 8.4$ kpc, $z_{\rm o}$ = 2.0 kpc, $R_{\rm max}$ = 18–20 kpc, so that the total old disk luminosity is 1.2 10^9 $L_\odot$. The old disk now contains only 7% of the total light in old stars. The larger value for $z_{\rm o}$ than is usual among disks in later type spirals is likely to be a result of the dominance of the gravitational field of the rounder bulge, even in the plane of the disk.

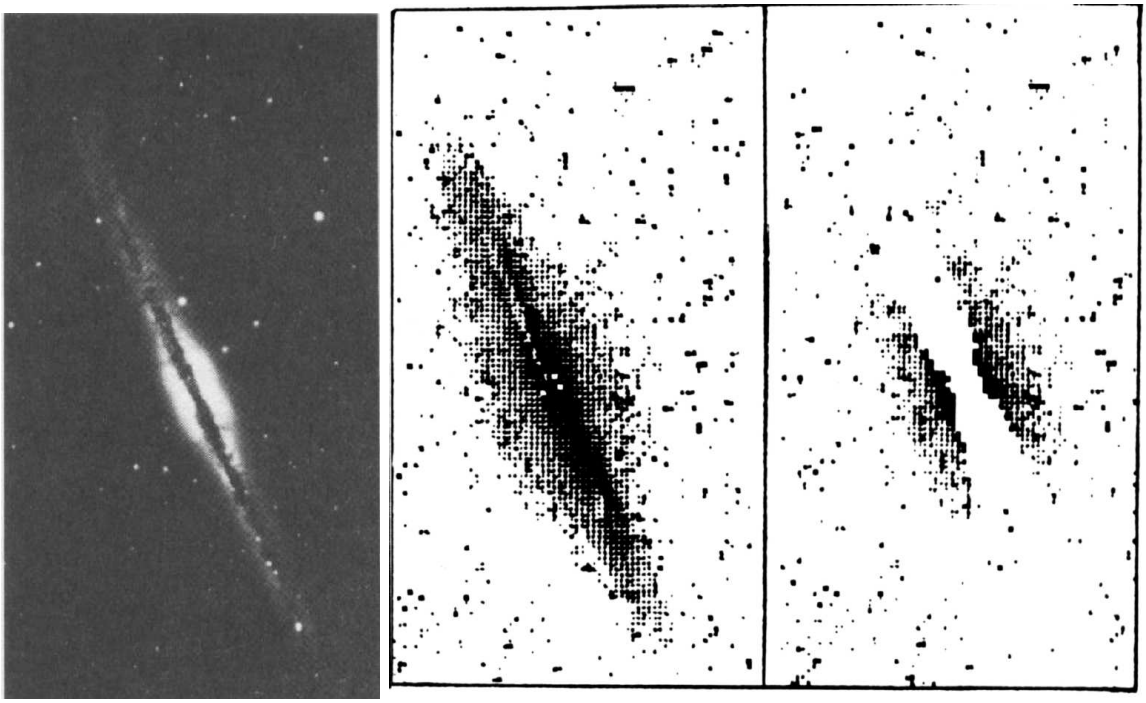

Figure 5.10: Grey-scale representation of the color distribution in NGC 891. The range of colors is from about $(U-V) = 0.6$ (light) to 1.4 (black). At the left is the total galaxy light and at the right that of the bulge after disk subtraction. After van der Kruit and Searle (1981b).

The color distribution in the bulge shows again a progressive bluing with radius, but is remarkable in the sense that the isochromes have the same shape as the isophotes. The observed range is $(U-B) = 0.6$ to 0.3 and $(B-V) = 1.3$ to 0.5 with the same uncertainties as for NGC 891. The magnitude of the variation is again that observed among Galactic globular clusters. The disk colors are very uncertain and are about $(U-B) = 0.6$, $(B-V) = 1.1$, again within the uncertainties consistent with an old disk population. As was also the case in NGC 891, the minor axis profiles can in three observed colors be fitted rather well with $R^{1/4}$-laws, albeit with different slopes as a function of wavelength.

The general inference that can be drawn from this work is that the light distributions in spiral galaxies can apparently be described very well with only two basic components: a bulge and a disk. These two basic components have two discretely different flattenings. In the bulge we furthermore have found evidence for color gradients, which are interpreted as abundance gradients, and this is a feature that appears typical for bulges (see Wirth and Shaw, 1983). Disks on the other hand are in general uniform in color with galactocentric distance. In this course, a considerable body of evidence will be presented that

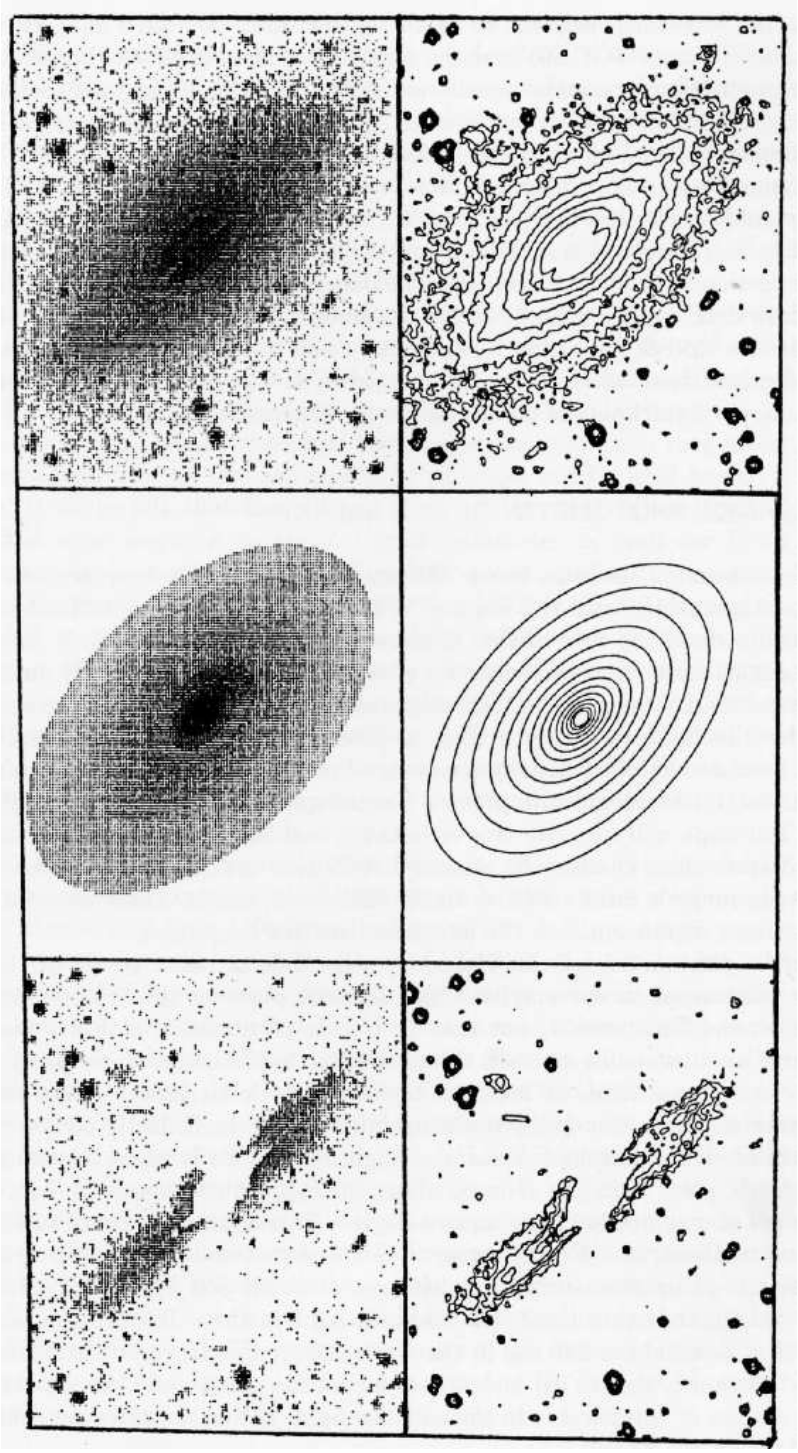

Figure 5.11: Illustration of the component decomposition of NGC 7814, at the right as isophotes and at the left in intensity grey-scale. The faintest isophote is at about 26 mag arcsec^{-2} and the interval is 0.5 mag. At the top we have again the total light and in the middle is the model for the bulge. This model has an $R^{1/4}$ luminosity profile and the isophotes have constant flattening. The bottom pictures show the disk remaining after subtraction of the bulge model from the observations. After van der Kruit and Searle (1982b).

points to a third component, intermediate between disk and halo in flattening, metallicity and kinematics, sometimes referred to as the "thick disk". Detailed analysis of the photometric data of NGC 891 (van der Kruit, 1984) shows that the bulge surface brightness distribution can equally well be represented by a bulge with somewhat changing axis ratio or a combination of a bulge with constant axis ratio and a component rather similar to the "thick disk" proposed for our Galaxy. On the other hand, we find no evidence whatsoever of such a component in NGC 7814. My personal view is, that this leaves unaffected the basic conclusion from fig. 5.6, that after disk subtraction we have a stellar distribution that has a characteristic flattening that is noticeably less than in the disk. Furthermore, in our Galaxy the "thick disk" makes up only about 10% or so of the disk light, and if associated with disk formation it can equally well be seen as a subcomponent of the disk population, which after all goes down at the other side of the range of flattenings to a thickness of about 100 pc for extreme Population I.

5.5 Surface photometry of our Galaxy

The distribution of the stars in our Galaxy has traditionally been studied using star counts, starting with the work of William Herschel two centuries ago and around the turn of the century of Kapteyn and others. It would be of obvious interest to supplement this work with surface photometry analogous to that in external systems. In particular this would allow a much better determination of the disk scalelength than is possible with currently available star counts. This is so, because at present all-sky counts are limited to stars brighter than about magnitude 11 (the program to provide a catalogue of guide stars for the Hubble Space Telescope will improve this situation) and faint counts are available in selected area's only, while the general distribution of stars in the intermediate magnitude range is most sensitive to the disk scalelength. These relevant stars do contribute significantly to the integrated surface brightness.

Surface photometry of the Galaxy is very difficult as a result of the low surface brightness, except maybe in the galactic plane or the brighter parts of the bulge and because it is not easy to obtain photometric stability over the very large angular scales involved. From

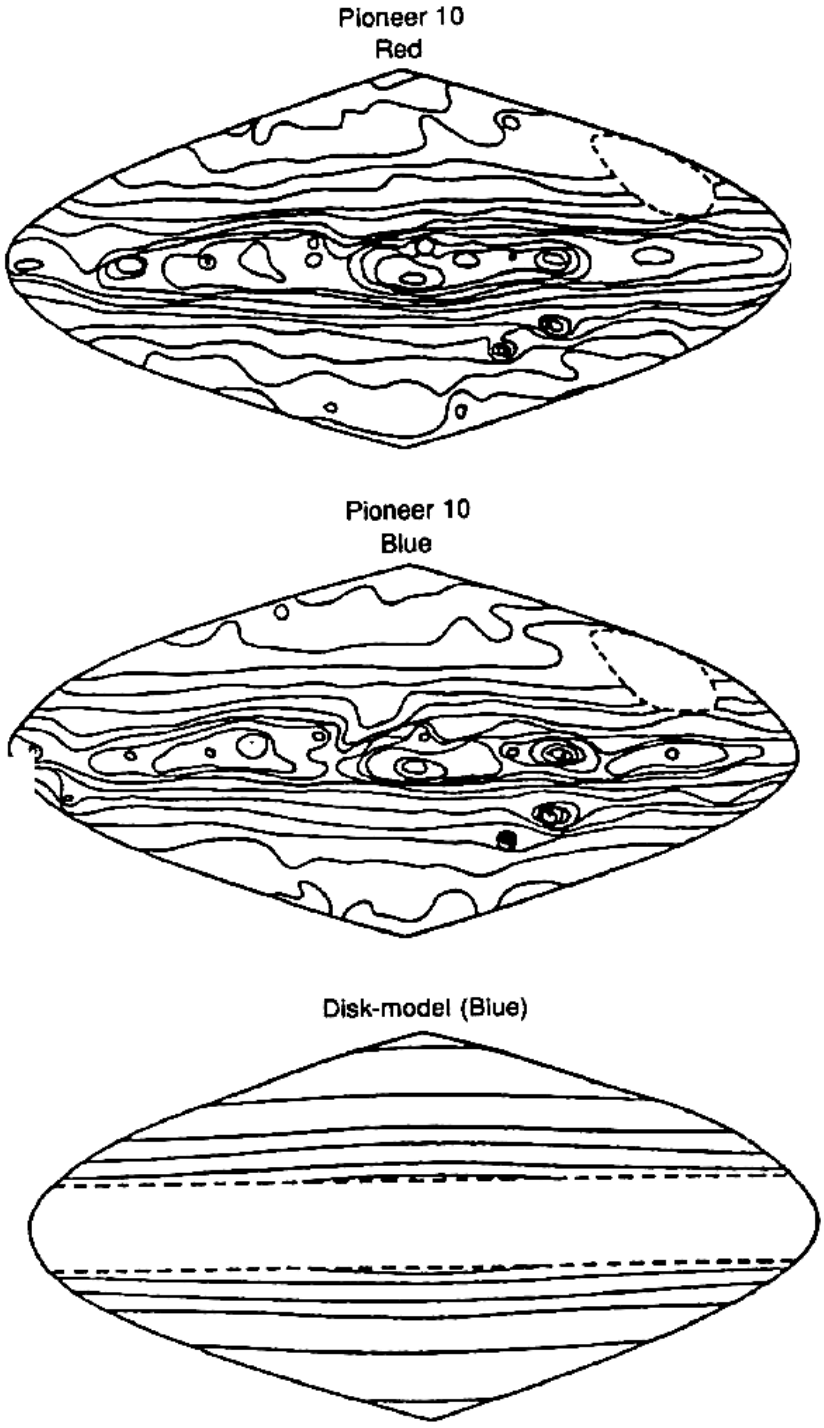
Pioneer 10
Red
Pioneer 10
Blue
Disk-model (Blue)

Figure 5.12: Isophote maps of the distribution of surface brightness from the integrated starlight from our Galaxy, as derived by Pioneer 10 on its way to and beyond Jupiter. Stars brighter than $m_V = 6.5$ have been removed. The direction toward the Galactic Center is in the middle of the picture. The angular resolution is 8° and the contour interval is 0.25 mag. In the red band the faintest thick contour corresponds to 24 V-mag arcsec^{-2} and in the blue band to 24 B-mag arcsec^{-2}. The missing part is the general direction of the sun as seen from Jupiter around Pioneer 10 encounter. The Galactic bulge, Carina spiral arm region and the Magellanic Clouds are prominent. From van der Kruit (1986).

the earth furthermore one has to worry about the zodiacal light, at least for higher galactic latitudes, where due to absence of absorption the interesting information on Galactic structure can be obtained. For example, the surface brightness of the integrated starlight in the galactic poles is in the B-band about 30 S_{10}, which means the equivalent of 30 stars of magnitude 10 per square degree. This is in units more familiar to us equal to about 24.8 B-mag arcsec^{-2}. For comparison, the brightest parts of the Galactic plane have surface brightnesses of about 800 S_{10} (about 21.2 mag arcsec^{-2}). On the other hand, the zodiacal light in the ecliptic poles provides about 80 S_{10} and about 210 S_{10} in the "Gegenschein" directly opposite to the sun on the sky. Obviously the (to us) interesting part of the integrated galactic starlight is fainter or comparable to the zodiacal light and is therefore very difficult to study from the earth.

Now fortunately the inverse problem occurs for researchers of the zodiacal light itself, for whom the galactic background light is a nuisance. Therefore, the Pioneer 10 (and 11) spacecraft, that were sent to Jupiter and were equipped with a wide-field mapping capability in the optical, were used to study this matter. Beyond the asteroid belt it turned out that there was no perceptible zodiacal light visible (except of course in directions near to that of the sun) and the spacecraft was then used on its continuing journey to and beyond Jupiter to map the background starlight in particular to assist in zodiacal light studies from the earth. The instrument used for this was a 1–inch telescope and an imaging photopolarimeter that in the configuration used provided a field of view of $2° \times 7°$. After many repeated scans this data resulted in two maps of the sky in the red and the blue with an angular resolution of 2°. Many scans remain unreduced and only a set from Pioneer 10 are available. After smoothing to an angular resolution of 8° the maps in fig. 5.12 result, presented there as isophotes maps in mag arcsec^{-2}.

Positional data by themselves can in principle not be used to derive lengthscales. It turns out that the Pioneer data can be used to constrain the ratio of radial scalelength h to vertical scale parameter z_o (van der Kruit, 1986). Estimates for z_o can be obtained from star count studies towards the galactic poles. Of course, the area's of high extinction

($E(B-V) > 0.09$ mag) have been excluded, restricting the analysis essentially to latitudes above about 20°. The exclusion of low latitudes is the reason that the ratio of scalelength to the solar galactocentric radius cannot be extracted from the data. It turns out also that the bulge is too faint to contribute sufficiently for a detailed study. The method to analyze the Pioneer data (van der Kruit, 1986) has been to use the Bahcall and Soniera (1984) computer code to derive surface brightnesses for various combinations of lengthscales.

The major result then is a definite value for the ratio h/z_o of 8.5±1.3. Using the value for the exponential old disk scaleheight in the solar neighborhood from Gilmore and Reid (1983) and others of 350±50 pc, which equals $0.5z_o$, results then in a radial scalelength h of the disk of 5.5±1.0 kpc. There are various other, independent arguments that can be used to derive values for h and I have concluded from a detailed discussion of these that the best value is 5.0±0.5 kpc (van der Kruit, 1987b). Other results of the Pioneer 10 data are the central surface brightness of the Galactic disk (now the total disk and not the old disk population only), inferred from the surface brightness at the galactic poles and this value for the scalelength, of 22.1±0.3 B-mag arcsec^{-2} and the color index of the disk at the solar position of $(B-V) = 0.84\pm0.15$. The latter is interestingly red and may indicate that the contribution from young population I to the surface brightness is not the major one. It may be untypical for the disk in general, although Sb galaxies do have disks with similar colors. The uncertainty of 0.15 mag is large, but can in principle be improved using the unreduced data from Pioneer 10 and 11. The total luminosity of the disk is (1.8±0.3) 10^{10} $L_\odot$. For the old disk the value of L(0,0) is about 5 10^{-2} $L_\odot$ pc^{-3} and the total luminosity is about 1 10^{10} $L_\odot$.

The value for $R_{\rm max}$ of the disk of the Galaxy is more difficult to derive. Young stars are observed in the anticenter direction to galactocentric distances of at least 22 kpc (Chromey, 1979), while a similar distance is found for HII regions. This gives an estimate for $R_{\rm max}$ of 20–25 kpc, in agreement with the observed ratio's $R_{\rm max}/h$ of 4.2±0.6 in external edge-on galaxies.

Surface photometry of the bulge has been attempted photoelectrically by de Vaucouleurs and Pence (1978) and has been successful in the brighter parts at low latitudes. They compared the projected surface brightness on the sky to that of an $R^{1/4}$-bulge and came up with the values $R_e = 2.7$ kpc and $\mu_o = 15.1$ B-mag arcsec^{-2}. From comparison with external galaxies we can estimate a value for the flattening from the kinematics, using the relation between V_m/σ and the flattening, where V_m is the maximum rotation velocity of the bulge and σ the central velocity dispersion (Kormendy and Illingworth, 1982). Current best values are $V_m = 60\pm30$ km s^{-1} and $\sigma = 110\pm10$ km s^{-1} (e.g. Freeman, 1987) and lead to $b/a = 0.7\pm0.15$. The total luminosity then is about 3 10^9 $L_\odot$. The old disk population contains about 80% of the total light in old stars, comparable to the number for NGC 891.

At another point in these lectures, I will discuss in more detail the statistical dis-

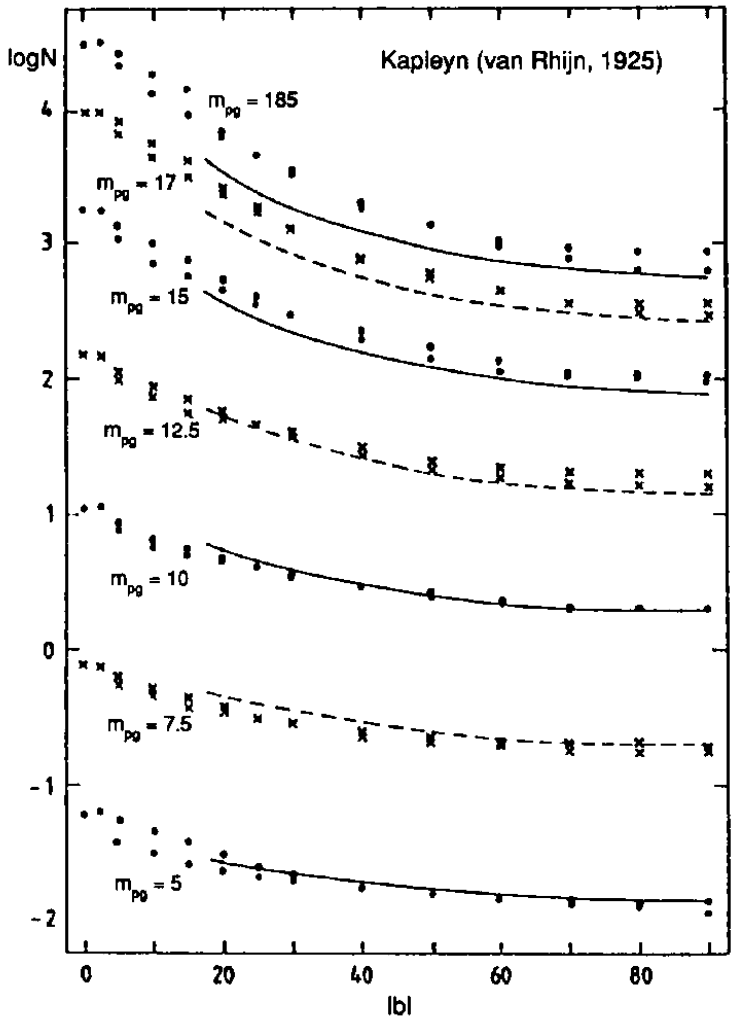

Figure 5.13: Comparison of the Kapteyn star counts in the Selected Area's reported in van Rhijn (1925) to the model of the Galaxy with the parameters derived in this section. The two values at each position come from positive and negative latitudes. From van der Kruit (1986).

tribution of luminosity parameters, especially those of the disks. At this stage I want to make two remarks. The first is that the photometric parameters of our Galaxy are rather similar to those of NGC 891, which is classified as Sb. This similarity is discussed more extensively in van der Kruit (1984). The scalelength of the disk of M31 is slightly larger, namely 6.0±0.5 kpc (Walterbos and Kennicutt, 1987). The second point is that

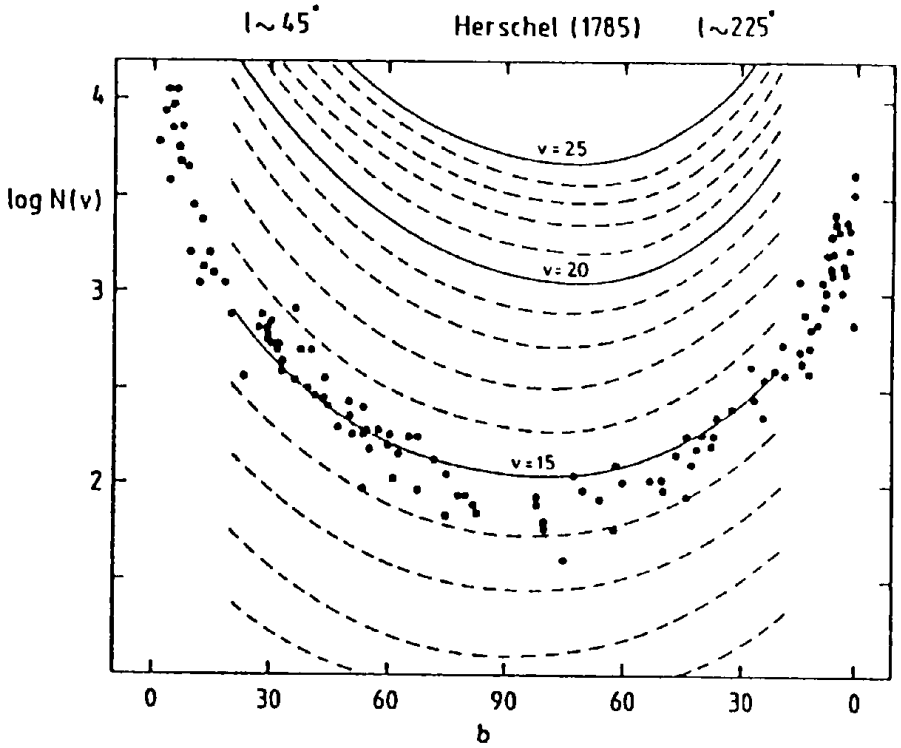

Figure 5.14: Comparison of the star counts made by Herschel (1785) to predictions from the Galaxy model with the parameters in this section. This great circle crosses the Galactic plane at longitudes about 45° and 225° and misses the poles by about 5°. Herschel counted stars to a limiting magnitude V of about 15. From van der Kruit (1986).

we can use these data to constrain the Hubble constant by comparing these values to those for the largest spirals in the Virgo cluster (van der Kruit, 1986; photometry by Watanabe, 1983). The six largest Sb galaxies in the Virgo cluster have a scalelength of 52±5 arcsec and the five largest Sc galaxies 50±5 arcsec. If our Galaxy is comparable to these systems the distance to the Virgo cluster would be 20±3 Mpc (from Sb galaxies) or 21±3 Mpc (Sc galaxies), using $h = 5.0 \pm 0.5$ kpc. The scalelength of M31 leads to 24±3 Mpc. For a distance of 22±4 Mpc with $V_{\rm rad}$(Virgo) = 1000±50 km s^{-1} and a Local Group infall of 330±40 km s^{-1} this results in a Hubble constant $H_{\rm o}$ of 65±10 km s^{-1} Mpc^{-1}. Comparing our Galaxy and M31 to galaxies with smaller scalelengths results of course in smaller values for $H_{\rm o}$. We see already that these two galaxies in the Local Group probably rank among the largest spirals in the Local Supercluster. A Hubble constant of 100 km s^{-1} Mpc^{-1} makes these probably the two largest in this volume, a very unlikely and unsatisfactory result.

It is an interesting fact that the surface brightness of the background integrated starlight is almost entirely (for more than 99%) provided by the stars brighter than magnitude 20 or so. In fact, before the Pioneer measurements this was the way in which it was estimated (e.g. Roach and Megill, 1961), using the extensive work earlier this century on the Plan of Selected Area's (e.g. van Rhijn, 1925). The difficulty was, however, that the old magnitude scales were unreliable. For historical purposes it is of interest to see just how reliable these are. This can be checked by calculating the star counts from a Bahcall and Soniera type model of the stellar distribution in the Galaxy, using the parameters for h, z_o and the local disk luminosity function as given above in agreement with the Pioneer surface brightness. In fig. 5.13 various counts predicted from the model are compared with the ones given by van Rhijn (1925) as a function of latitude at a number of magnitudes. From this figure it is obvious that the scales go systematically wrong at fainter magnitudes in the sense that the estimated magnitudes by van Rhijn are too bright. The difference amounts to 1/2 to 3/4 of a magnitude at the limits of the counts. It is true, however that the counts are very consistent as a guide to relative variations that result from the stellar distribution in space.

It is also of interest to compare the model for the Galaxy with the counts that Herschel made two centuries ago. The necessary information can be found in the paper by Herschel (1785), where he publishes his famous cross-cut of the "Sidereal System". In his analysis he assumed that his telescope was able to see all the way to the edges of the Sidereal System and that therefore the number of stars seen in a particular part of the sky could be used to calculate the distance of this edge in that direction. The procedure, how to work back from this cross-cut is described in more detail in van der Kruit (1986). The result is given in fig. 5.14, where we can see that Herschel observed consistently to a limiting magnitude V of about 15. This is a remarkable achievement.

5.6 References

Bahcall, J.N., Soniera, R.M. 1984, Astrophys. J. Suppl. **55**, 67
Begeman, K. 1987, Ph. D. Thesis, Univ. of Groningen
Binney, J. 1982, Monthly Notices Roy. Astron. Soc. **200**, 951
Chromey, F.R. 1979, Astron. J. **84**, 534
de Vaucouleurs, G. 1948, Ann. d'Astrophys. **11**, 247
de Vaucouleurs, G. 1959a, Handbuch der Physik **53**, 511
de Vaucouleurs, G. 1959b, Astrophys. J. **127**, 487
de Vaucouleurs, G., Pence, W.D. 1978, Astron. J. **83**, 1163
Freeman, K.C. 1970, Astrophys. J. **160**, 811
Freeman, K.C. 1987, Ann. Rev. Astron. Astrophys. **25**, 603

Gilmore, G., Reid, N. 1983, Monthly Notices Roy. Astron. Soc. **202**, 33
Herschel, W. 1785, Phil. Trans. LXXV, 213
Jaffe, W. 1983, Monthly Notices Roy. Astron. Soc. **202**, 995
Jarvis, B.J., Freeman, K.C. 1985a, Astrophys. J. **295**, 314
Jarvis, B.J., Freeman, K.C. 1985b, Astrophys. J. **295**, 324
Kent, S. 1987, Astron. J. **93**, 816
King, I.R. 1966, Astron. J. **71**, 64
Kormendy, J. 1982, in: Morphology and Dynamics of Galaxies, Saas-fee course 1982, Geneva Observatory
Kormendy, J., Illingworth, G. 1982, Astrophys. J. **256**, 460
Okamura, S. 1988, Publ. Astron. Soc. Pacific **100**, 524
Patterson, F.S. 1940, Harvard Bull. No. 914, p. 9
Reynolds, R.H. 1913, Monthly Notices Roy. Astron. Soc. **74**, 132
Rhijn, P.J. van 1925, Publ. Groningen Astron. Obs. No. 43
Roach, F.E., Megill, L.R. 1961, Astrophys. J. **133**, 228
Schombert, J.M., Bothun, G.D. 1987, Astron. J. **92**, 60
Shostak, G.S., van der Kruit, P.C. 1984, Astron. Astrophys. **132**, 20
van der Kruit, P.C. 1979, Astron. Astrophys. Suppl. **38**, 15
van der Kruit, P.C. 1984, Astron. Astrophys. **140**, 470
van der Kruit, P.C. 1986, Astron. Astrophys. **157**, 230
van der Kruit, P.C. 1987a, Astron. Astrophys. **173**, 59
van der Kruit, P.C. 1987b, in: The Galaxy, ed. G. Gilmore & B. Carswell, Dordrecht: Reidel, p. 27
van der Kruit, P.C. 1988, Astron. Astrophys. **192**, 117
van der Kruit, P.C., Searle, L. 1981a, Astron. Astrophys. **95**, 105
van der Kruit, P.C., Searle, L. 1981b, Astron. Astrophys. **95**, 116
van der Kruit, P.C., Searle, L. 1982a, Astron. Astrophys. **110**, 61
van der Kruit, P.C., Searle, L. 1982b, Astron. Astrophys. **110**, 79
Walterbos, R., Kennicutt, R.C. 1987, Astron. Astrophys. **198**, 61
Watanabe, H. 1983, Annals Tokyo Obs., 2nd Ser. **19**, 121
Wevers. B.M.H.R. 1984, Ph. D. Thesis, Univ. of Groningen
Wevers, B.M.H.R., van der Kruit, P.C., Allen, R.J. 1986, Astron. Astrophys. Suppl. **66**, 505
Wielen, R. 1977, Astron. Astrophys. **60**, 263
Wilson, C.P. 1975, Astron. J. **80**, 175
Wirth, A., Shaw, R. 1983, Astron. J. **88**, 171
Young, P. 1976, Astron. J. **81**, 807